JCTC Journal of Chemical Theory and Computation

On the Validation of Molecular Dynamics Simulations of Saturated and *cis*-Monounsaturated Phosphatidylcholine Lipid Bilayers: A Comparison with Experiment

David Poger*,† and Alan E. Mark†,‡

School of Chemistry and Molecular Biosciences and Institute for Molecular Bioscience, University of Queensland, Brisbane St Lucia, QLD 4072, Australia

Received September 15, 2009

Abstract: Molecular dynamics simulations of fully hydrated pure bilayers of four widely studied phospholipids, 1,2-dilauroyl-*sn*-glycero-3-phosphocholine (DLPC), 1,2-dimyristoyl-*sn*-glycero-3-phosphocholine (DMPC), 1,2-dioleoyl-*sn*-glycero-3-phosphocholine (DOPC), and 2-oleoyl-1-palmitoyl-*sn*-glycero-3-phosphocholine (POPC) using a recent revision of the GROMOS96 force field are reported. It is shown that the force field reproduces the structure and the hydration of bilayers formed by each of the four lipids with high accuracy. Specifically, the solvation and the orientation of the dipole of the phosphocholine headgroup and of the ester carbonyls show that the structure of the primary hydration shell in the simulations closely matches experimental findings. This work highlights the need to reproduce a broad range of properties beyond the area per lipid, which is poorly defined experimentally, and to consider the effect of system size and sampling times well beyond those commonly used.

1. Introduction

Pure phospholipid bilayers have been extensively studied as models for biomembranes.[1,2] Although lipids may exhibit a wide diversity of phases (such as the gel and liquid-crystalline phases), the most biologically relevant state under physiological conditions is the fluid phase (alternatively named the liquid crystal, L_α phase or, more correctly, the liquid-disordered phase L_d) in which the lipid chains are flexible and disordered. The fluidity of membranes precludes the accurate determination of their structure at an atomic level.[1] As a consequence, theoretical techniques, especially molecular dynamics (MD) simulations, have contributed greatly to our understanding of the structure and the dynamical properties of membrane systems as well as to the interpretation of experimental results. The basic features of the mechanisms of fundamental processes, such as vesicle formation[3] and fusion,[4] peptide-induced[5,6] and peptide-free[7] pore formation, ion permeation through membranes,[8−12] lipid flip-flop,[13,14] spontaneous lipid aggregation into a bilayer,[15] and formation of gel[16] and ripple[17] phases, have been modeled using MD simulations.

The quality and the validity of the results from such MD simulation studies depend heavily on the fidelity with which the underlying model, or force field, used describes the interatomic interactions. Biomolecular force fields are being continuously improved and updated. Currently, the most widely used force fields for lipid systems are the all-atom CHARMM[18,19] and the united-atom GROMOS96[20] force fields and the parameter set proposed by Berger et al.[21] The latest revision of the GROMOS96 force field (parameter set 53A6)[22] was based on the reproduction of the solvation properties (free enthalpies of hydration) of small molecule analogues of biomolecules. The G53A6 parameter set has been extensively studied and validated for the simulation of peptides, proteins and DNA in water.[23,24] However, it failed to reproduce the properties of phosphatidylcholine lipids—a major component of biological membranes—in the fluid phase.[25] We recently reported a correction of the G53A6 parameter set ($G53A6_L$), which greatly improved the fluidity of 1,2-dipalmitoyl-*sn*-glycero-3-phosphocholine (DPPC) lipid bilayers.[25] Specifically, the repulsion between the choline methyl groups and the nonester phosphate oxygens was

* E-mail: d.poger@uq.edu.au.
† School of Chemistry and Molecular Biosciences.
‡ Institute for Molecular Bioscience.

10.1021/ct900487a
Published on Web 11/23/2009

Table 1. Summary of Published Areas Per Lipid A_L (in nm^2) Measured in Experiments and in Simulations in Fluid-Phase DLPC, DMPC, DPPC, DOPC and POPC Bilayers[a]

source	lipid bilayer				
	DLPC	DMPC	DPPC	DOPC	POPC
Experiment					
	0.69 (RT)[94]	0.58 (297)[95]	0.665 (317)[96]	0.70 (275)[97]	0.54 (275)[98]
	0.665 (293)[96]	0.67 (298)[99]	0.625 (318)[100]	0.82 (RT)[94]	0.63 (297)[95]
	0.572 (293)[101]	0.652 (300)[102]	0.643 (318)[100]	0.594 (296)[103]	0.683 (303)[48]
	0.594 (295)[104]	0.65 (300)[94]	0.57 (323)[105]	0.82 (298)[102]	0.66 (310)[106]
	0.687 (298)[102]	0.595 (303)[107]	0.712 (323)[102]	0.718 (298)[100]	0.62 (323)[98]
	0.71 (298)[99]	0.597 (303)[108]	0.69 (323)[99]	0.726 (298)[100]	
	0.626 (303)[65]	0.596 (303)[1]	0.71 (323)[94]	0.722 (303)[60]	
	0.632 (303)[47]	0.60 (303)[65]	0.717 (323)[109]	0.725 (303)[1]	
		0.660 (303)[28]	0.629 (323)[110]	0.721 (303)[32]	
		0.589 (303)[111]	0.633 (323)[65]	0.724 (303)[48]	
		0.606 (303)[47]	0.64 (323)[1]	0.674 (303)[29]	
		0.657 (309)[96]	0.642 (323)[64]	0.724 (303)[30]	
		0.600 (309)[101]	0.628 (323)[29]		
		0.622 (310)[104]	0.631 (323)[29]		
			0.695 (338)[104]		
Simulation literature	0.629 (303)[27][b]	0.577 (300)[112][d]	0.61 (323)[21][c]	0.651 (303)[38][c]	0.693 (298)[26][b]
	0.630 (303)[27][b]	0.577 (300)[113][d]	0.62 (323)[15][c]	0.65 (310)[87][f]	0.655 (300)[114][h]
	0.660 (323)[115][c]	0.618 (303)[27][b]	0.635 (323)[116][c]	0.658 (303)[27][b]	0.668 (303)[117][f]
		0.621 (303)[27][b]	0.66 (323)[118][c]	0.660 (303)[27][b]	
		0.592 (305)[119][e]	0.636 (323)[27][b]		
		0.602 (310)[120][b]	0.637 (323)[27][b]		
		0.558 (310)[87][f]	0.60−0.64 (325)[121][b]		
		0.625 (314)[26][b]	0.691 (325)[122][c]		
		0.611−0.635 (323)[37][c]	0.50−0.57 (325)[123][b]		
		0.656 (323)[124][c]	0.604 (325)[125][b]		
		0.57 (325)[86][b]	0.645 (325)[125][g]		
			0.623 (325)[26][b]		
			0.65 (350)[126][c]		
G53a6$_L$	0.632 (303)	0.616 (323)	0.631 (323)[25]	0.649 (303)	0.638 (303)

[a] Temperatures (in K) are indicated in parentheses (room temperature,RT). The data are presented in a chronological order for each temperature. [b−h] The force field parameter sets used in simulations are: [b] as described in the reference; [c] Berger parameters;[21] [d] AMBER94;[33] [e] CHARMM22;[36] [f] GAFF;[34] [g] CHARMM27;[19] and [h] CHARMM19[35] (partial charges from CHARMM22[36]).

enhanced by increasing the van der Waals radius of the atom of oxygens for this particular interaction. The structural properties of these bilayers (area and volume per lipid, electron density profiles, bilayer thickness and hydration, ordering and conformation of acyl chains) were in very good agreement with experiment. The self-assembly of DPPC into a bilayer in water was also simulated, demonstrating that a bilayer is the thermodynamically preferred state.

Two recently developed lipid force fields include alternative GROMOS96-derived parameter sets. In the parameter set proposed by Kukol[26] and based on the GROMOS 53A6 parameter set, the repulsion between DPPC molecules was enhanced by increasing the van der Waals radius of the two carbonyl carbons in the glycerol moiety. This new parameter set was used to model various phospholipid bilayers in a fluid phase, and it was found that the area per lipid (A_L) was reproduced correctly for 1,2-dimyristoyl-*sn*-glycero-3-phosphocholine (DMPC), 2-oleoyl-1-palmitoyl-*sn*-glycero-3-phosphocholine (POPC), and DPPC and for simulations up to 40 ns. In contrast, Chiu et al.[27] partly reparameterized the GROMOS96 43a1 parameter set, specifically the bond and the van der Waals parameters. The new parameter set called 43a1-S3 was used to simulate pure lipid bilayers of 1,2-lauroyl-*sn*-glycero-3-phosphocholine (DLPC), 1,2-dioleoyl-*sn*-glycero-3-phosphocholine (DOPC), DMPC or DPPC in the fluid phase. The structural parameters of the bilayers calculated from the simulations, such as the area and the volume per lipid, the bilayer thickness, the deuterium order parameters, and the form factor, were in good agreement with experiment.

A_L is often used as the primary target property in the validation of lipid force field parameters to assess their ability to reproduce the correct phase of a membrane. However, there is considerable uncertainty in regard to the true value of A_L for a given lipid bilayer in the fluid phase.[1] In the last two decades, values of A_L derived from X-ray methods, NMR, and neutron diffraction have varied dramatically. For example, as shown in Table 1, in the case of the DMPC L_α phase, values of A_L as low as 0.596 nm^2 [1] and as high as 0.660 nm^2 [28] have been proposed in the last nine years. Similarly, recent values of A_L for the L_α phase of DOPC, published even by the same group of authors, range from 0.674 nm^2 [29] to 0.724 nm^2 [30] at 303 K. One reason for the scatter in the values of A_L obtained experimentally is that the area per lipid is frequently not measured directly but inferred from other quantities, such as order parameters from NMR spectroscopy.[31] Fluctuations in the structure of lipid bilayers, which are inherent in the bilayer being in a fluid phase, also make the accurate determination of this structural quantity difficult.[32]

In contrast, the areas per lipid obtained in simulations appearing in the literature fall in a narrow range, regardless of the parameter set used (such as Berger,[21] GROMOS,[20] AMBER[33,34] or CHARMM)[18,19,35,36] and regardless of whether the simulations required or not the application of a surface tension to reproduce a value of the area per lipid compatible with a fluid bilayer. They are also seemingly independent of the length of the simulation and the extent to which the specific system was equilibrated. This is surprising as structural relaxation times in bilayer systems can be long (>100 ns) and, even at equilibrium, the area per lipid in simulations of systems (including relatively small ones) under periodic boundary conditions can fluctuate on a time scale of tens of nanoseconds.[37−39] The uniformity in the values from simulations is all the more striking given the variation in the methodology used, such as the method for the treatment of the long-range electrostatic interactions (particle mesh Ewald,[40,41] reaction field,[42] straight cutoff, or shift function).[43] Furthermore, corrections for the effects of undulations in the membrane and other artifacts inherent in the quantity measured experimentally are rarely—if ever—considered. Instead A_L is normally determined simply as the area of the simulation box divided by the number of lipids, not by modeling the experiment. It is also noteworthy that a reasonable agreement of a value of A_L obtained from simulations with experiment can be misleading. For example, a value of 0.56 nm^2 was found when simulating a hydrated DPPC bilayer with the original GROMOS 53A6 force field.[25] Despite this value being considered low, it is still almost within the range of experimental values listed in Table 1 (0.57−0.717 nm^2). However, other properties, such as the electron density profile across the bilayer, were characteristic of bilayers in a gel-like phase. The simulation of hydrated DLPC, DMPC, and POPC bilayers with the original GROMOS 53A6 force field showed a similar behavior (data not shown). Therefore, the ability of a parameter set to model a fluid bilayer must be judged based on a combination of several properties and not only on the area per lipid.

In this work, the ability of the G53A6$_L$ parameter set to reproduce the structural and hydration properties of pure bilayers of DLPC, DMPC, DOPC, and POPC in a L_α phase is examined. Together with DPPC bilayers, these phospholipids bilayers have been best characterized experimentally.[1,44] The myristoyl, oleoyl and palmitoyl acyl chains are also among the major fatty tails found in biologically relevant phospholipids.[45] For example, POPC is the most abundant lipid in animal cells.[46] The results from the simulations are compared to a wide range of structural properties (including the area and volume per lipid, the isothermal area compressibility modulus, the bilayer thickness, the deuterium order parameters, and the conformation of the acyl chains as well as the orientation and hydration of the headgroups and the carbonyls). The results demonstrate that the G53A6$_L$ parameter set is well suited for simulating a range of phosphatidylcholine lipids in the fluid phase. In addition, by collecting and tabulating the range of experimental results that have been obtained for these properties experimentally, we not only provide a measure of the uncertainty in these values but also underline the need to validate models against a range of properties, in contrast to just a specific value of, for example, the area per lipid.

2. Methods

2.1. Simulation Systems. Four different systems were simulated. Each system consisted of a pure lipid bilayer containing either DLPC (12:0/12:0), DMPC (14:0/14:0), DOPC (18:1c9/18:1c9), or POPC (16:0/18:1c9). The lipids were described using the recently derived GROMOS 53A6 parameter set for phosphatidylcholines (G53A6$_L$).[25] Each system consisted of a hydrated 128-lipid bilayer (64 lipids in each leaflet) initially constructed by replicating a pair of lipids on an 8 × 8 grid. The area per lipid for each membrane was set initially to the experimentally measured area per lipid of the appropriate bilayer in the L_α phase. The areas per lipid used were 0.632 nm^2 for DLPC,[47] 0.606 nm^2 for DMPC,[47] 0.724 nm^2 for DOPC,[30] and 0.683 nm^2 for POPC.[48] Sufficient water molecules were added to give the desired level of hydration for fluid bilayers (with a ratio of 35−40 H_2O per lipid).

2.2. Simulation Parameters. All simulations were performed using the GROMACS package, version 3.2.1[49] under periodic boundary conditions in a rectangular box. The temperature of the system was maintained by independently coupling the lipids and the solvent to an external temperature bath at the reference temperature of 303 K with a coupling constant τ_T of 0.1 ps using a Berendsen thermostat.[50] The temperature for each system (303 K) was chosen above the gel→liquid-crystalline phase transition temperature (276.4, 296.9, 255.7, and 270.5 K for DLPC, DMPC, DOPC and POPC, respectively[51−54]). The pressure was kept at 1 bar in the lateral and normal directions by weakly coupling to a semi-isotropic pressure bath,[50] using an isothermal compressibility of 4.6×10^{-5} bar^{-1} and a coupling constant τ_P of 1 ps. Covalent bond lengths in the lipid were constrained using the LINCS algorithm.[55] The geometry of the simple point charge (SPC) water molecules[56] was constrained using SETTLE.[57] A 2-fs time step was used. Nonbonded interactions were evaluated using a twin-range cutoff scheme: interactions within the 0.8-nm short-range cutoff were calculated every step, whereas interactions within the 1.4-nm long-range cutoff were updated every 5 steps together with the pair list. A reaction-field correction was applied to the electrostatic interactions beyond the long-range cutoff[42] using a relative dielectric permittivity constant of 62, as appropriate for SPC water.[58] The force field parameters (G53A6$_L$) used to calculate the inter- and intramolecular interactions in lipids have been described previously.[25] This parameter set was derived from the GROMOS 53A6 force field.[22] Specifically, the repulsion between the choline methyls and the nonester phosphate oxygens was enhanced.

Each system was initially energy-minimized and then simulated at 50 K for 10 ps. The temperature was then increased gradually over 100 ps until the final simulation temperature was reached. Each system was simulated twice. The equilibration of the systems was monitored by examining the time evolution of the potential energy and the area per lipid of the system. Once the systems were equilibrated, data

Table 2. Overview of the Systems Simulated

lipid bilayer	total time (ns)	sampling time (ns)
DLPC	220, 350	120
DMPC	235, 245	120
DOPC	260, 300	120
POPC	245, 250	120

were collected for 120 ns. An overview of the simulations performed is given in Table 2.

3. Results

3.1. Area and Volume Per Lipid and Isothermal Area Compressibility Modulus. The area A_L per lipid was calculated from the lateral dimensions of the simulation box divided by the number of lipids in each leaflet. A_L is often used to judge the convergence of simulations of lipid bilayers. Similarly, the volume per lipid V_L was calculated by subtracting the volume occupied by the water molecules from the volume V of the simulation box:

$$V_L = \frac{V - n_w V_w}{n_L} \quad (1)$$

where n_L and n_w are the number of lipid (128) and water molecules, respectively. V_w is the volume per water molecule. V_w was determined from an independent 15-ns simulation of 1 728 SPC water molecules at 303 K and at a pressure of 1 bar. The value of V_w obtained was 3.09×10^{-2} nm^3. The average values of A_L and V_L from the simulations are reported in Table 3 together with the values obtained experimentally. As found previously in regard to DPPC, the G53A6 force field[25] yields are in good agreement with experiment for both properties for each of the systems simulated (DLPC, DMPC, DOPC, and POPC). The A_L's calculated from the simulations are in general agreement with the experimental values measured for fluid bilayers listed in Table 1. The simulated values of V_L fall within less than 2% of the experimental values.

The isothermal area compressibility modulus K_A is related to the fluctuations of A_L:

$$K_A = \frac{2k_B\langle T\rangle\langle A_L\rangle}{n_L \sigma_A^2} \quad (2)$$

where k_B is the Boltzmann constant, $\langle T\rangle$ is the average temperature, $\langle A_L\rangle$ is the average area per lipid and σ_A^2 is the variance associated to A_L. The average area compressibility moduli calculated from the simulations are given in Table 3, along with the alternative experimental values of 234 ± 23 for DMPC,[59] 188,[60] 254,[30] 265 ± 18[59] for DOPC, and 180−330 mN·m^{-1}[61] for POPC in the fluid phase. As previously found in the case of the simulation of a fluid DPPC bilayer with the G53A6$_L$ parameter set,[25] the values of K_A derived from the simulations are about a factor of 2 larger than the experimental values. Nonetheless, they are consistent with previous estimates of K_A obtained from simulation studies, which were in the range of 200−600 mN·m^{-1}.[37,43] The discrepancy with experiment is mainly due to the values of σ_A^2 being low, which leads to an overestimation of K_A.[37,62]

3.2. Electron Density Profiles. The structure of the bilayers was compared with the available X-ray scattering data by calculating an electronic density profile from the simulations. Ideally, one would directly compare the simulation and experimental data in reciprocal space but, to make the comparison direct, the spacing of the layers in the simulations would have to match those in the experiment exactly. Alternatively, the electron density profiles across the bilayer for DLPC, DMPC, DOPC, and POPC shown in Figure 1 are a straightforward, common way to compare qualitatively with experiment. The two main peaks in the density profiles are due to the phosphorus atoms, the most electron-dense atoms in the bilayers. The bilayer thickness can be characterized in several ways. The thickness D_{HH} of a bilayer is commonly taken as the distance between the two phosphate peaks. Alternatively, the Luzzati thickness D_B is defined as[1]

Table 3. Summary of Structural Properties of Bilayers at Equilibrium Measured in Experiments and in the Simulations[a]

lipid bilayer	A_L (nm^2)	V_L (nm^3)	K_A (mN·m^{-1})	D_{HH} (nm)	D_B (nm)
DLPC					
experiment	0.54−0.71[b]	0.991[47]	—	3.08[47]	3.14[47]
simulation	0.632 (3)	0.969 (1)	461 (96)	2.85 (1)	3.07 (4)
DMPC					
experiment	0.58−0.67[b]	1.0955[28] 1.101[1,47]	234 (23)[59]	3.44[108] 3.53[47] 3.60[1]	3.63[47] 3.69[1,108]
simulation	0.616 (1)	1.077 (1)	475 (10)	3.27 (3)	3.49 (3)
DOPC					
experiment	0.594−0.82[b]	1.303[1,29,30,48,60]	188[60] 254[30] 265 (18)[59]	3.53[60] 3.67[29,30] 3.69[1] 3.71[32]	3.59[1] 3.61[32,60] 3.87[29]
simulation	0.649 (2)	1.284 (1)	389 (19)	3.63 (2)	3.89 (1)
POPC					
experiment	0.54−0.683[b]	1.223[98] 1.256[48]	180−330[61]	3.70[48]	3.68[48]
simulation	0.638 (4)	1.232 (1)	404 (55)	3.46 (4)	3.87 (1)

[a] A_L, area per lipid; V_L, volume per lipid; K_A, isothermal area compressibility modulus; D_{HH}, bilayer thickness; D_B, Luzzati bilayer thickness. The numbers in parentheses are error estimates in the last digit(s) of the averages.
[b] See Table 1.

$$D_B = b_z - \int_{-b_z/2}^{b_z/2} \rho_w(z)dz \quad (3)$$

where b_z is the z-dimension of the simulation box and $\rho_w(z)$ is the probability distribution of water along z. $\rho_w(z)$ was calculated from the time-averaged histogram of the distribution of water along the z-axis with a bin width of dz:

$$\rho_w(z) = \frac{n_w(z)V_w}{dV} \quad (4)$$

where $n_w(z)$ is the time-averaged number of water molecules per slice and dV is the time-averaged volume of a slice.[27] The values of D_{HH} and D_B observed in the simulations are reported in Table 3. Again, the values calculated are consistent with the values obtained from experimental studies of lipid bilayers in the fluid phase. D_{HH} and D_B values obtained in the simulations are within 9% of those measured experimentally and are listed in Table 3.

The decomposition of the overall electron density into the contributions from different groups—namely water, choline moieties (Cho), phosphate groups (P), glycerol and carbonyls

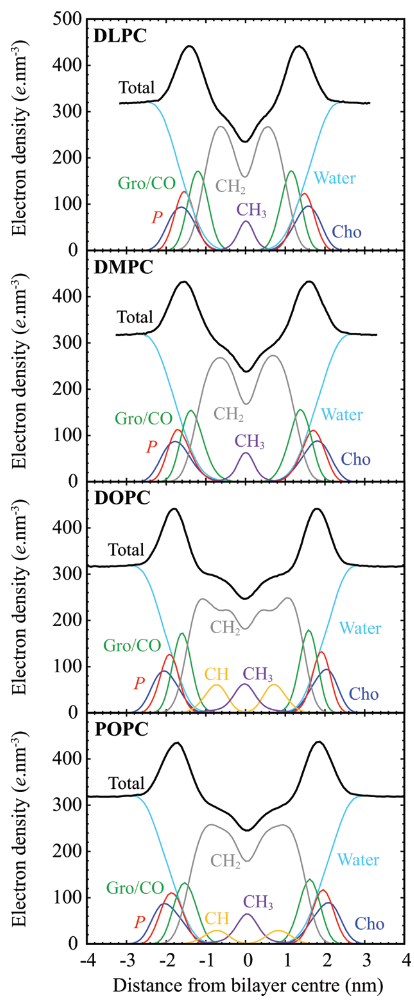

Figure 1. Electron density profiles of the whole hydrated DLPC, DMPC, DOPC, and POPC bilayers and of the contribution of their individual components (Cho: contribution from the choline moieties; P: phosphate groups; Gro/CO: contribution of the glycerol and carbonyl groups; CH_2: methylenes of the acyl chains; CH: CH=CH groups in the oleoyl chains; CH_3: terminal methyls of the acyl chains).

groups (Gro/CO), methylenes (CH_2) and terminal methyls (CH_3) of the acyl chains, and CH=CH groups in the oleoyl chains of DOPC and POPC (CH)—are also presented in Figure 1. The profiles are relatively symmetric, indicating that the bilayers are equilibrated. Water was found to penetrate into the bilayers up to the Gro/CO groups,[63] while the terminal methyl groups in the acyl chains were dehydrated, in agreement with experiment.[47,48,64]

3.3. Ordering of the Acyl Chains. The deuterium order parameters S_{CD} of the lauroyl (Lau), myristoyl (Myr), palmitoyl (Pam), and oleoyl (Ole) acyl chains, in the simulations of DLPC, DMPC, DOPC, and POPC, were calculated and compared to the available experimental data. S_{CD} measures the relative orientation of the C—D bonds with respect to the bilayer normal. The order parameter S_{CD} of a methylene group is defined as

$$S_{CD} = \frac{1}{2}\langle 3\cos^2\theta - 1\rangle \quad (5)$$

where θ is the angle between a C—D bond of the methylene in the given acyl chain and the normal to the bilayer (z -axis). The angular brackets indicate an ensemble average. As the GROMOS force field uses an united-atom representation, the positions of the deuterons were constructed based on the positions of the neighboring carbons assuming tetrahedral geometry. The $|S_{CD}|$ profiles of the lipid *sn*-1 and *sn*-2 acyl chains of DLPC, DMPC, DOPC, and POPC, together with various experimental profiles based on NMR measurements, are presented in Figure 2. In all cases, the $|S_{CD}|$ values are lower than 0.25, which indicates than the aliphatic chains are disordered. The variation in $|S_{CD}|$ and in the magnitudes for the DLPC and DMPC bilayers are very similar to the values of Petrache et al.[65] and Douliez et al.[66] obtained experimentally. There is some discrepancy for the methylenes 2 and 3 in the Lau tails, but Douliez et al.[66] reported that the $|S_{CD}|$ for the second methylene could not be determined accurately.

In the case of POPC, the simulations reproduced the differences between the $|S_{CD}|$ values of the *sn*-1 Pam and *sn*-2 Ole chains observed experimentally.[67−69] The *sn*-1 Pam chain shows a continuous decrease in $|S_{CD}|$ characteristic of saturated chains. In contrast, the profile of the *sn*-2 Ole chain has a distinctive dip, corresponding to the double bond between carbons 9 and 10. The *sn*-2 Ole chain is also clearly less ordered than the saturated chain.[68,69] To our knowledge, no experimental values of $|S_{CD}|$ for the oleoyl chains in DOPC have been published. However, the two Ole tails show similar variations to the $|S_{CD}|$ of *sn*-2 Ole in POPC, as expected.

3.4. Conformation of Acyl Chains. Another structural parameter that can be inferred from experiment is the preference for given rotamers and sequences of rotamers in the acyl chains. Fourier transform infrared (FTIR) spectroscopy can be used to determine the number of *trans* (t) and *gauche* (g) conformers in an acyl chain and the sequences of t and g (end *gauche eg*, *gg*, *gtg* and kinks *gtg′*). The combinations observed are characteristic of a given lipid phase with, for example, the gel-to-fluid phase transition being associated with an increase in the number of *gauche* conformers and of kinks in the acyl chains.[70−72] In the simulations of DLPC, DMPC, DOPC, and POPC, the torsion

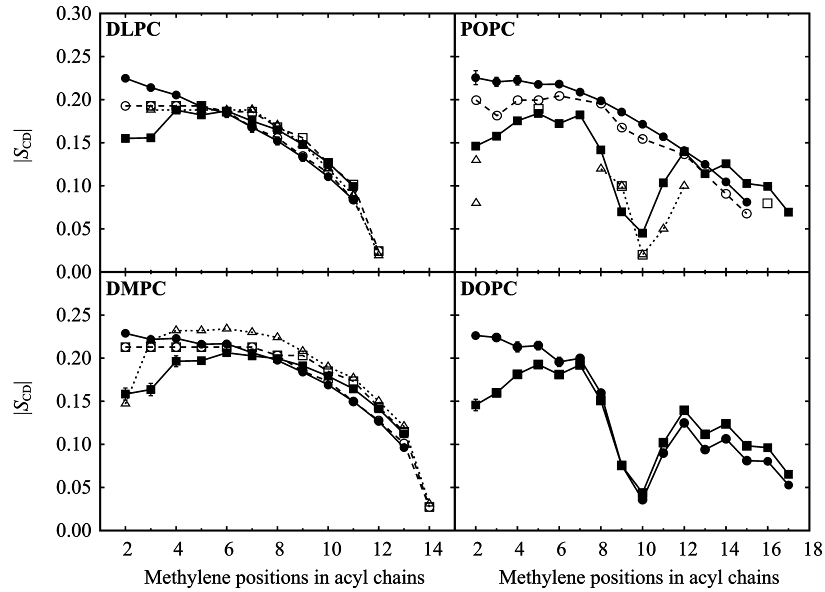

Figure 2. Deuterium order parameter $|S_{CD}|$ profiles of the *sn*-1 (●) and *sn*-2 (□) fatty acyl chains of hydrated DLPC, DMPC, DOPC, and POPC bilayers calculated from the simulations (Lau, 12:0; Myr, 14:0; Pam, 16:0; and Ole, 18:1c9). The $|S_{CD}|$ values are averaged over all the lipid *sn*-1 and -2 acyl chains in the systems and over the two simulations. Experimental $|S_{CD}|$ values: for DLPC and DMPC, $|S_{CD}|$ measured by Petrache et al.[65] for the *sn*-1 (○) and *sn*-2 (□) acyl chains; for DLPC, *sn*-2 Lau at 308 K from Douliez et al.[66] (△); for DMPC, *sn*-2 Myr from Douliez et al.[66] (△); for POPC, *sn*-1 Pam from Seelig and Seelig at 300 K[67] (○), *sn*-2 Ole from Perly et al.[69] (□), and from Seelig and Waespe-Šarčević[68] (△).

Table 4. Occurrence of Rotamer Sequences in Acyl Chains (*eg*, *gg*, *gtg′*, and *gtg′* + *gtg*) Estimated from Experiment and in the Simulations[a]

	number of bonds or bond sequences per chain								
	experiment					simulation			
rotamer	DLPC[74]	DMPC[76]	DPPC	DPPE[75]	POPE[75]	DLPC	DMPC	DOPC	POPC
eg	0.45	0.38	0.54[74] 0.38[76] 0.4[75]	0.1	0.05	0.34 (1)	0.31 (0)	0.31 (0)	0.31 (0)
gg	0.32	0.67	0.40[74] 0.57[76] 0.4[75]	0.2	0.2	0.37 (0)	0.50 (0)	0.41 (0)	0.45 (0)
gtg′	0.88[b]	—	1.19[74 b]	—	—	0.29 (0)	0.36 (1)	0.31 (0)	0.37 (0)
gtg′ + *gtg*	—	0.44	0.46[76] 1.0[75]	1.0	0.8	0.56 (0)	0.66 (0)	0.59 (0)	0.69 (1)

[a] The numbers between the parentheses are error estimates in the last digit of the averages. [b] The *gtg′* sequence may be ascribed to a *gtg′* + *gtg* sequence.[72]

angles ϕ in the acyl chains were classified as t ($\phi < -150°$ or $\phi > 150°$), g^- ($-90° \le \phi < -30°$) or g^+ ($30° < \phi \le 90°$).[73] The results are listed in Table 4 together with the available experimental values.[74−76] The estimates of *eg* and *gg* from the simulations of DLPC and DMPC are in good agreement with experiment. As noted previously in regard to DPPC,[25] apparent discrepancies for *gtg′* and *gtg* + *gtg′* are due mainly to experimental uncertainties in the assignment of *gtg* and *gtg′* methylene wagging modes.[72] No experimental data is available for DOPC and POPC. Nevertheless, given the experimental data available for phosphatidylcholines and phosphatidylethanolamines shown in Table 4, it is possible to judge the quality of the simulations of the DOPC and POPC bilayers. As is evident from Table 4, experimentally, there are marked differences in the incidence of specific rotameric sequences between DPPC (0.38−0.54 *eg*,[74−76] 0.40−0.57 *gg*,[74−76] and 0.46−1.0 *gtg′* + *gtg*[75,76] per palmitoyl chain) and DPPE (0.1 *eg*, 0.2 *gg*, and 1.0 *gtg′* + *gtg*)[75] in the L_α phase. By comparing the propensity of palmitoyl chains to have *eg*, *gg*, and *gtg′* + *gtg* rotamers in DPPC and DPPE bilayers in the fluid phase, Senak et al.[75] estimated there were gains of 0.3−0.4 in *eg*, 0.2 in *gg*, and 0.1 in *gtg′* + *gtg* per chain going from a DPPC to a DPPE bilayer. By extrapolating their observations to fluid POPC and POPE bilayers, the number of *eg*, *gg*, and *gtg′* + *gtg* rotamer sequences per acyl chain, calculated from the simulation of a POPC bilayer (0.31 *eg*, 0.45 *gg*, and 0.69 *gtg′* + *gtg*), seems consistent with those obtained experimentally from a POPE bilayer in the L_α phase (0.05 *eg*, 0.2 *gg*, and 0.8 *gtg′* + *gtg*).[75]

No experimental values for DOPC were found, but the trend observed in the simulation of a DOPC fluid bilayer is similar to that of POPC, with a higher population of kinks

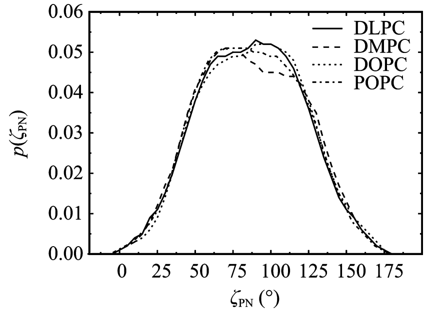

Figure 3. Probability distribution function of the angle ζ_{PN} between the bilayer normal pointing away from the middle of the bilayer to bulk water and the lipid headgroup $P^{-} \rightarrow N^{+}$ vectors in the simulations of DLPC, DMPC, DOPC, and POPC.

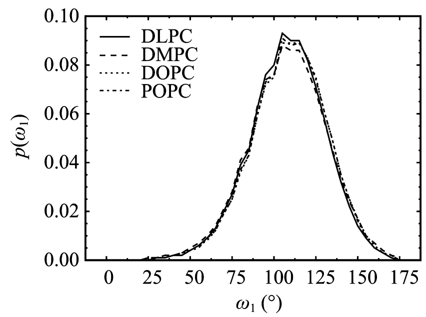

Figure 4. Probability distribution function of the angle ω_1 between the bilayer normal pointing away from the middle of the bilayer to bulk water and the *sn*-1 carbonyl O→C vectors in the simulations of DLPC, DMPC, DOPC and POPC.

+ *gtg* than that of *eg* and *gg* sequences, as previously noticed by Chia and Mendelsohn.[77]

3.5. Orientation of the Headgroups and of the Carbonyls. Büldt et al.[78] have shown that the dipole moment along the $P^{-} \rightarrow N^{+}$ vector in the phosphocholine headgroup lies almost parallel to the surface of the membrane. Figure 3 shows the probability distribution function of the angle ζ_{PN} between the $P^{-} \rightarrow N^{+}$ dipole and the outward bilayer normal. The distributions of ζ_{PN} obtained from the simulations of DLPC, DMPC, DOPC, and POPC are similar with most probable angles ζ_{PN} being 88°, 87°, 91°, and 86°, respectively. Accordingly, the headgroups, on average, lie nearly parallel to the bilayer surface.

The orientation of the *sn*-1 and -2 carbonyl $O^{\delta-} \rightarrow C^{\delta+}$ dipoles with respect to the outward bilayer normal was also calculated (angles ω_1 and ω_2, respectively). The probability distributions of ω_1 and ω_2 are shown in Figures 4 and 5, respectively. Again, the distributions are similar in all systems, with the most probable value for the angle ω_1 being 107° for DLPC, DMPC, DOPC, and POPC. The most probable value of ω_2 was 132°, 127°, 132°, and 135° for DLPC, DMPC, DOPC, and POPC, respectively.

3.6. Hydration of the Headgroups and Glycerol/Carbonyls Moieties. The distribution of the water molecules around the atoms within the headgroup, the glycerol group as well as the *sn*-1 and *sn*-2 carbonyls, were calculated. Figure 6 illustrates the distribution of the distance between the oxygens of water and the nearest phosphocholine headgroup atom in the simulations of DLPC, DMPC, DOPC,

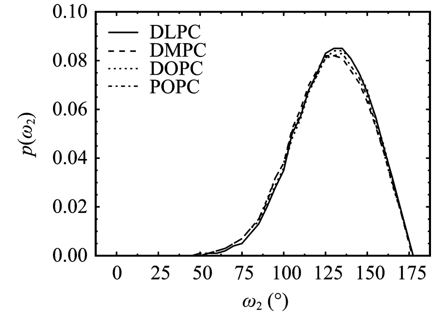

Figure 5. Probability distribution function of the angle ω_2 between the bilayer normal pointing away from the middle of the bilayer to bulk water and the *sn*-2 carbonyl O→C vectors in the simulations of DLPC, DMPC, DOPC, and POPC.

and POPC. The curves obtained in all simulations are essentially identical with three peaks at 0.27, 0.34, and 0.63 nm, indicating that the interaction of water with the headgroups does not depend upon the nature of the lipid tails. The integration of the distributions up to the second peak shows that there are 14.5, 14.3, 14.9, and 14.9 water molecules per lipid headgroup for DLPC, DMPC, DOPC, and POPC, respectively (Table 5). These results are in accord with experiment from which a ratio of about 11−20 water molecules per lipid in a fluid phase has been estimated.[79−82] The decomposition of the distributions of *P*Cho into the individual contributions of the choline (Cho) and phosphate (*P*) groups, together with the distributions of the water oxygens to the nearest glycerol (Gro), *sn*-1 carbonyl (CO^{sn-1}) and -2 carbonyl (CO^{sn-2}) groups are depicted in Figure 7. All four bilayers show similar distributions with a distinct first peak at 0.34 nm for Cho, 0.28 nm for *P*, 0.29 nm for Gro, 0.27 nm for CO^{sn-1}, and 0.26 nm for CO^{sn-2}. *P* and Gro also have a clear second peak at 0.47 and 0.38 nm, respectively. As listed in Table 5, it was found that there were, on average, 13−14 water molecules around the choline groups at 0.34 nm, about 3 and 10−11 water molecules around phosphates at 0.28 and 0.47 nm, respectively, and 1.6 water molecules around the carbonyls at the *sn*-2 positions at 0.26 nm. Despite the presence of a peak at 0.29 nm for Gro and at 0.27 nm for CO^{sn-1}, the integration of the peaks shows that they correspond to less than one water molecule on average.

4. Discussion

Overall, the GROMOS 53A6 force field parameters have been shown to be effective in representing a range of phosphatidylcholine lipids in a fluid phase and are able to reproduce a range of structural properties, such as the area per lipid, the volume per lipid, the deuterium order parameters, the hydration properties in close agreement with experiment, and, to a lesser extent, the isothermal compressibility modulus. The validation of simulation studies of membranes in a fluid phase is, however, a difficult task. Phospholipids are amphipathic molecules with the central polar glycerol group bound to one or two long, hydrophobic acyl chains and to a polar or charged headgroup. As a consequence, the phase behavior of a lipid bilayer is the result of a subtle balance between inter- and intramolecular

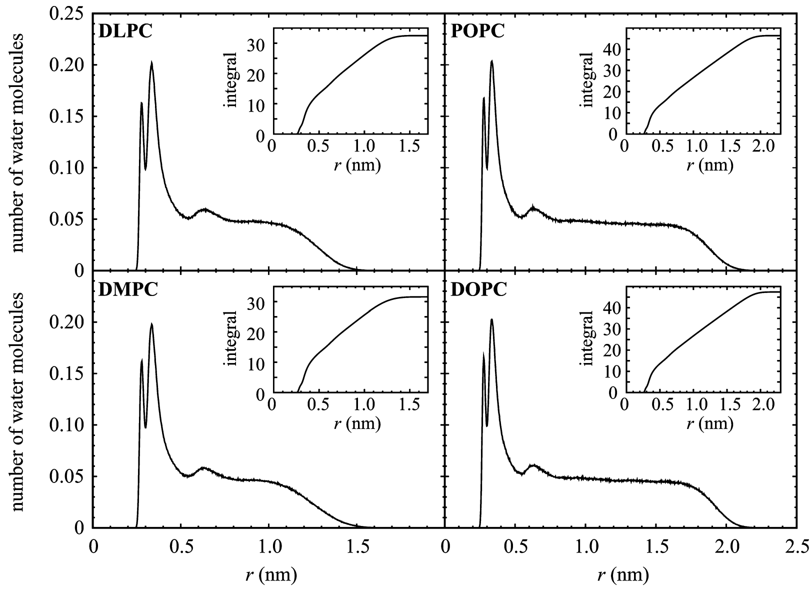

Figure 6. Distribution of the distance between the oxygen of water and the nearest lipid headgroup atom in the simulations of DLPC, DMPC, DOPC, and POPC. Insets: Integral of the distribution.

Table 5. Number of Water Molecules Per Lipid Hydrating the Phosphocholine Headgroup and the Different Polar Moieties in Lipids[a]

	number of water molecules per group					
lipid bilayer	*P*Cho	Cho	*P*	Gro	$CO^{sn\text{-}1}$	$CO^{sn\text{-}2}$
DLPC	2.6	13.5	3.2	0.2	0.6	1.6
	14.5		10.2	3.3		
DMPC	2.5	13.3	3.3	0.2	0.6	1.6
	14.3		10.3	3.5		
DOPC	2.6	14.0	3.2	0.2	0.6	1.6
	14.9		10.9	3.4		
POPC	2.7	13.6	3.3	0.2	0.6	1.6
	14.9		10.9	3.3		

[a] Phosphocholine (*P*Cho), choline (Cho), phosphate (*P*), glycerol (Gro), and carbonyls at the *sn*-1 (CO^{sn-1}) and *sn*-2 (CO^{sn-2}) positions. The values correspond to the integration up to the first peak in the distribution of water in Figure 6 for *P*Cho and in Figure 7 for the other groups. In the case of *P*Cho, *P* and Gro, the second values correspond to the integration up to the second peak.

interactions[83] as well as the balance between interactions within the headgroup and tail regions. The compactness of a bilayer also means that structure and dynamics are strongly correlated. For example, in a gel phase, lipids pack more closely and are more highly ordered than in a L_α phase. The degree of ordering is often estimated by the area per lipid A_L, but this is generally measured indirectly, and the range of alternative experimental values is broad (see Table 1). In simulations, A_L is dependent on the sampling time, the size of the system, and the methodology used.[37−39,43] As a result, A_L is just one of a range of properties that need to be considered during the validation of force field parameters for lipids. In this work, a range of structural properties (A_L, bilayer thicknesses D_{HH} and D_B, S_{CD}, conformation of the acyl chains, and orientation of the headgroups) were used to validate the G53A6 parameter set. As shown in Table 3 and Figure 2, a good agreement was found with experiment not only for A_L but also for all the structural properties investigated. Although high, the estimates obtained for the isothermal area compressibility modulus in all the bilayers (within the range of 389−475 mN·m^{-1}, see Table 3) are consistent with the range of 200−600 mN·m^{-1} obtained in previous simulation studies by Anézo et al.[43] This said, it must be noted that the Berendsen weak-coupling method[50] was used in both studies to maintain constant temperature and pressure, which might account for the discrepancy. The Berendsen thermostat and barostat do not give rise to an exact *NPT* ensemble. In particular, the weak-coupling method can suppress short-time fluctuations in the temperature and the pressure even though the long-time averages are correct. In this regard, it should be stressed that, while the fluctuations in the temperature and the pressure in the simulations occur on a 1−10-ps time scale, the fluctuations in A_L occur on a 10−100 ns time scale. Thus, fluctuations in A_L are not expected to be strongly affected or biaised by the relaxation time used in the weak coupling of temperature ($\tau_T = 0.1$ ps) and pressure ($\tau_P = 1$ ps). Other factors that could lead to an underestimation of the fluctuations in A_L include the suppression of the fluctuations due to the small size of the system and/or the time scale over which the fluctuations were accumulated. To determine the extent to which the values of K_A reflect the size of the system and the length of the sampling time, two additional simulations of a POPC bilayer at equilibrium with 361 lipids per leaflet were performed under the same conditions described in Section 2, the Methods section. The variation in K_A as a function of the extent of sampling time for the POPC bilayers in the fluid phase containing either 64 or 361 lipids per leaflet is shown in Figure 8. It is evident in Figure 8 that the apparent value of K_A depends strongly on both the size of the system simulated and the time scale over which σ_A^2 is determined; the value of K_A becoming closer to experiment the longer the sampling time or the larger the bilayer for a fixed sampling time. For example, with a sampling time of 60 ns, K_A is almost a factor of 2 lower in the bilayer comprising 361 POPC per leaflet ($K_A = 454 \pm 89$ mN·m^{-1}) than in the

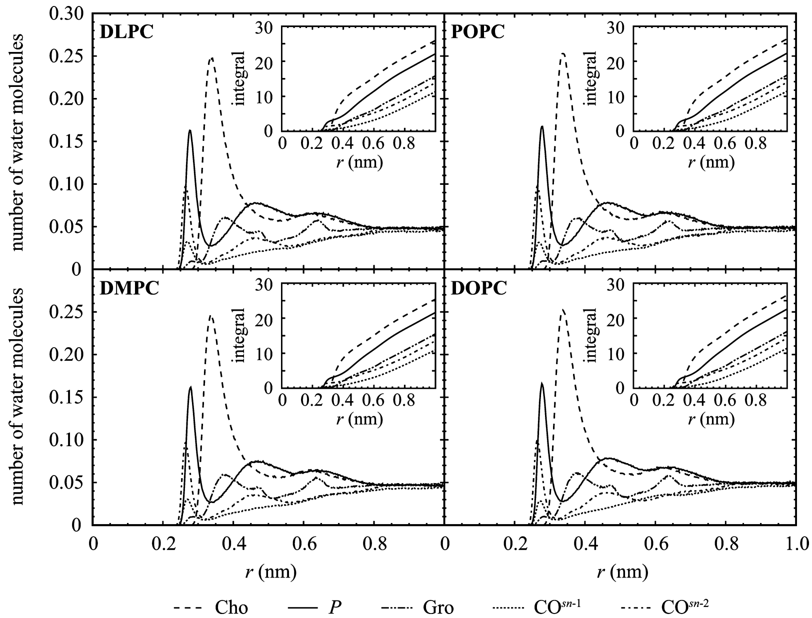

Figure 7. Distribution of the distance between the oxygen of water and the nearest atom of the choline (Cho), phosphate (*P*), glycerol (Gro), *sn*-1 (CO^{sn-1}), and *sn*-2 (CO^{sn-2}) carbonyl groups in the simulations of DLPC, DMPC, DOPC, and POPC. Insets: Integrals of the distributions.

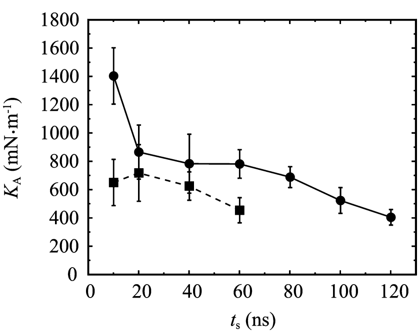

Figure 8. Isothermal area compressibility modulus K_A calculated over different sampling times t_s from the simulations of a fluid POPC bilayer comprising 64 (●) or 361 (■) lipids per leaflet. For each value of t_s, the initial time t_i for sampling was determined using the total time of the simulation t_t such that $t_i = t_t - t_s$. The error bars show the standard deviation of the average K_A over two independent simulations for a given value of t_s for each system.

bilayer with 64 lipids per leaflet ($K_A = 781 \pm 101$ mN·m^{-1}). In both cases, the average value of A_L is consistent with experiment (0.638 nm^2 in the 361 lipid per leaflet bilayer and 0.630 nm^2 in the 64 lipid per leaflet bilayer). In the smaller system, variations of A_L due to undulatory and peristaltic (thickness fluctuations) motions in bilayers,[37] which determined the value of σ_A^2 used in eq 2, were occurring on a time scale of 50−100 ns. This accounts for the decrease in K_A with increased sampling. In the larger system which contained almost six times the number of lipids per leaflet, the value of σ_A^2 converged more rapidly as expected. Note that the error bars shown in Figure 8 reflect the standard deviations of the average values of K_A calculated over the two independent equilibrium trajectories for a given sampling time. While in principle a larger bilayer is expected to reduce the effects of periodic boundary conditions and improve convergence, larger bilayers have the added complication that collective properties, such as the bending of the bilayer, must also be taken into account. In this case, alternative formulas to eq 2 must be used.[37] This underlines the need to consider not only a wide range of properties but also the effect of sampling time and of system size when validating models.

While the overall structural properties such as A_L are central to validating force field parameters, the local properties, such as the sequences of rotameric states or the interaction with interfacial water, are equally important. Hydration forces play a critical role in the structure of fluid lipid bilayers.[84,83] Chandrasekhar et al.[85] showed that the balance between the water−water, lipids−lipids, and interfacial water−lipids interactions is crucial to allow a sufficient number of water molecules to interact with headgroups. NMR spin−lattice relaxation measurements, as a function of lipid hydration, suggested a ratio of 11−16 H_2O per lipid,[79] and more specifically 14−20 water molecules per lipid in the case of DOPC, in a liquid crystalline phase.[80,81] Lairión et al.[82] estimated the number of interfacial waters to be 12−16 in reversed micelles. The first hydration shell of lipids corresponds to the first two peaks in Figure 6. Figure 7 shows that the phosphate and carbonyl groups mainly contribute to the inner peak, whereas the choline and glycerol moieties are to a greater extent responsible for the outer peak. The integration of the distributions of the distances of the water oxygens to the closest lipid headgroup in the simulations is illustrated in the insets in Figure 6. This shows that there are approximately 14−15 water molecules up to the second peak: 14.5, 14.3, 14.9, and 14.9 water molecules per headgroup for DLPC, DMPC, DOPC, and POPC, respectively (Table 5). This is in good agreement with the NMR results and with previous simulation studies on DMPC,[86,87] DPPC,[88] POPC,[89] and DOPC[87,89,90] fluid bilayers, for example. Note, the splitting of the first hydration shell into separate peaks for the phosphate and choline groups at 0.27

and 0.34 nm in the distribution function, in Figure 6, observed in all the simulations has been previously seen in simulations of DOPC[89,90] and POPC[89] performed with united-atom models (with peaks at approximately 0.25−0.27 and 0.32−0.36 nm) but not in the all-atom simulations of DMPC and DOPC by Rosso and Gould.[87] This highlights the extent to which local properties of a model may vary even if general properties, such as the area per lipid, are similar.

The two ester carbonyl groups are not equivalent in phospholipids. Infrared spectroscopic studies of fully hydrated DMPC bilayers[91,92] suggested that, whereas the *sn*-1 carbonyl is largely buried, the *sn*-2 carbonyl interacts strongly with water. In the simulations, similar features are found with CO^{sn-1} being almost desolvated, while CO^{sn-2} is bound to 1.6 water molecules on average (Table 5).

Polar and charged groups give rise to the existence of several dipoles in lipids, namely the $P^{-} \rightarrow N^{+}$ dipole in phosphocholines and the $O^{\delta-} \rightarrow C^{\delta+}$ dipoles of the *sn*-1 and *sn*-2 carbonyls, which show preferential orientations with respect to the surrounding water molecules. Using neutron diffraction, Büldt et al.[78] showed that the P−N dipole in phosphocholine headgroups lies almost parallel to the surface of the bilayer. Furthermore, the X-ray structure of DMPC dihydrate[93] shows that the *sn*-1 carbonyl lies flat in the plane of the bilayer, whereas the oxygen of the *sn*-2 carbonyl is directed toward water. Using the G53A6 parameter set, the appropriate orientation of the three dipoles was found consistent for all four lipid bilayers: the P−N dipole is parallel to the surface of the bilayer ($\zeta_{PN} \approx 90°$) and the dehydrated *sn*-1 carbonyl adopts a comparable orientation but with the O→C vector slightly pointing outward from the bilayer ($\omega_1 \approx 107°$), whereas the *sn*-2 carbonyl has its oxygen clearly directed toward water ($\omega_2 \approx 132°$).

5. Conclusion

The simulations of common phospholipids of varying length (DLPC and DMPC) and degree of saturation (DOPC and POPC) of the acyl chains demonstrate that the G53A6 parameter set is well suited for the simulation of phosphatidylcholine bilayers in the biologically relevant liquid-crystalline phase. The structural properties of the bilayers were validated using a broad range of experimental data for each lipid. Critically, the extent of hydration of the lipid headgroups was found to be in agreement with NMR, X-ray, and neutron diffraction as well as infrared spectroscopic data. The work underlines the fact that to validate simulation models, especially those used to model lipid bilayers, there is a critical need to examine a range of experimental data as opposed to focusing on a single parameter, such as the area per lipid in isolation.

Acknowledgment. This work was funded from the Australian Research Council (ARC). A.E.M. is an ARC Federation Fellow. All the calculations were performed using high-performance computing resources of the University of Queensland and the National Computational Infrastructure (NCI) National Facility at the Australian National University under the Merit Allocation Scheme through the Queensland Cyber Infrastructure Foundation (QCIF) partner share scheme.

Supporting Information Available: The topology files of the lipid molecules and the atomic coordinates of equilibrated fluid bilayers of DLPC, DMPC, DOPC, and POPC are provided. This information is available at http://compbio.chemistry.uq.edu.au/~david/research/lipids.htm and on the GROMOS Automated Topology Builder and Repository (http://compbio.chemistry.uq.edu.au/atb). This material is available free of charge via the Internet at http://pubs.acs.org.

References

(1) Nagle, J. F.; Tristram-Nagle, S. *Biochim. Biophys. Acta* **2000**, *1469*, 159–195.

(2) Vigh, L.; Escribá, P.; Sonnleitner, A.; Sonnleitner, M.; Piotto, S.; Maresca, B.; Horváth, I.; Harwood, J. L. *Prog. Lipid Res.* **2005**, *44*, 303–344.

(3) de Vries, A. H.; Mark, A. E.; Marrink, S.-J. *J. Am. Chem. Soc.* **2004**, *126*, 4488–4489.

(4) Marrink, S.-J.; Mark, A. E. *J. Am. Chem. Soc.* **2003**, *125*, 11144–11145.

(5) Leontiadou, H.; Mark, A. E.; Marrink, S.-J. *J. Am. Chem. Soc.* **2006**, *128*, 12156–12161.

(6) Sengupta, D.; Leontiadou, H.; Mark, A. E.; Marrink, S.-J. *Biochim. Biophys. Acta* **2008**, *1778*, 2308–2317.

(7) Leontiadou, H.; Mark, A. E.; Marrink, S.-J. *Biophys. J.* **2004**, *86*, 2156–2164.

(8) Marrink, S.-J.; Jähnig, F.; Berendsen, H. J. *Biophys. Chem.* **1996**, *71*, 632–647.

(9) Leontiadou, H.; Mark, A. E.; Marrink, S.-J. *Biophys. J.* **2007**, *92*, 4209–4215.

(10) Khavrutskii, I. V.; Gorfe, A. A.; Lu, B.; McCammon, J. A. *J. Am. Chem. Soc.* **2009**, *131*, 1706–1716.

(11) Vernier, P. T.; Ziegler, M. J.; Sun, Y.; Chang, W. V.; Gundersen, M. A.; Tieleman, D. P. *J. Am. Chem. Soc.* **2006**, *128*, 6288–6289.

(12) Gurtovenko, A. A.; Anwar, J. *J. Phys. Chem. B* **2007**, *111*, 10453–10460.

(13) Tieleman, D. P.; Marrink, S.-J. *J. Am. Chem. Soc.* **2006**, *128*, 12462–12467.

(14) Gurtovenko, A. A.; Vattulainen, I. *J. Phys. Chem. B* **2007**, *111*, 13554–13559.

(15) Marrink, S.-J.; Lindahl, E.; Edholm, O.; Mark, A. E. *J. Am. Chem. Soc.* **2001**, *123*, 8638–8639.

(16) Marrink, S.-J.; Risselada, J.; Mark, A. E. *Chem. Phys. Lipids* **2005**, *135*, 223–244.

(17) de Vries, A. H.; Yefimov, S.; Mark, A. E.; Marrink, S.-J *Proc. Natl. Acad. Sci. U.S.A.* **2005**, *102*, 5392–5396.

(18) MacKerell, A. D., Jr.; et al. *J. Phys. Chem. B* **1996**, *102*, 3586–3616.

(19) Feller, S. E.; MacKerell, A. D., Jr. *J. Phys. Chem. B* **2000**, *104*, 7510–7515.

(20) van Gunsteren, W. F.; Billeter, S. R.; Eising, A. A.; Hünenberger, P. H.; Krüger, P.; Mark, A. E.; Scott, W. R. P.; Tironi, I. G. *Biomolecular Simulation: The GROMOS96 Manual and User Guide*; vdf Hochschulverlag AG an der ETH Zürich and BIOMOS B.V.: Zürich, Switzerland, 1996.

(21) Berger, O.; Edholm, O.; Jähnig, F. *Biophys. J.* **1997**, *72*, 2002–2013.

(22) Oostenbrink, C.; Villa, A.; Mark, A. E.; van Gunsteren, W. F. *J. Comput. Chem.* **2004**, *25*, 1656–1676.

(23) Oostenbrink, C.; Soares, T. A.; van der Vegt, N. F.; van Gunsteren, W. F *Eur. Biophys. J.* **2005**, *34*, 273–284.

(24) Villa, A.; Fan, H.; Wassenaar, T.; Mark, A. E. *J. Phys. Chem. B* **2007**, *111*, 6015–6025.

(25) Poger, D.; van Gunsteren, W. F.; Mark, A. E. *J. Comput. Chem.* **2009**, In press (DOI: 10.1002/jcc.21396)

(26) Kukol, A. *J. Chem. Theory Comput.* **2009**, *5*, 615–626.

(27) Chiu, S.-W.; Pandit, S. A.; Scott, H. L.; Jakobsson, E. *J. Phys. Chem. B* **2009**, *113*, 2748–2763.

(28) Costigan, S. C.; Booth, P. J.; Templer, R. H. *Biochim. Biophys. Acta* **2000**, *1468*, 41–54.

(29) Kučerka, N.; Nagle, J. F.; Sachs, J. N.; Feller, S. E.; Pencer, J.; Jackson, A.; Katsaras, J. *Biophys. J.* **2008**, *95*, 2356–2367.

(30) Pan, J.; Tristram-; Nagle, S.; Kučerka, N.; Nagle, J. F. *Biophys. J.* **2008**, *94*, 117–124.

(31) van Gunsteren, W. F.; Dolenc, J.; Mark, A. E. *Curr. Opin. Struct. Biol.* **2008**, *18*, 149–153.

(32) Liu, Y.; Nagle, J. F. *Phys. Rev. E: Stat. Phys., Plasmas, Fluids, Relat. Interdiscip. Top.* **2004**, *69*, 040901.

(33) Cornell, W. D.; Cieplak, P.; Bayly, C. I.; Gould, I. R.; Merz, K. M.; Ferguson, D. M.; Spellmeyer, D. S.; Fox, T.; Caldwell, J. W.; Kollman, P. A. *J. Am. Chem. Soc.* **1995**, *117*, 5179–5197.

(34) Wang, J.; Wolf, R. M.; Caldwell, J. W.; Kollman, P. A.; Case, D. A. *J. Comput. Chem.* **2004**, *25*, 1157–1174.

(35) Brooks, B. R.; Bruccoleri, R. E.; Olafson, B. D.; States, D. J.; Swaminathan, S.; Karplus, M. *J. Comput. Chem.* **1983**, *4*, 187–217.

(36) MacKerell, A. D., Jr.; et al. *J. Phys. Chem. B* **1998**, *102*, 3586–3616.

(37) Lindahl, E.; Edholm, O *Biophys. J.* **2000**, *79*, 426–433.

(38) de Vries, A. H.; Mark, A. E.; Marrink, S.-J. *J. Phys. Chem. B* **2004**, *108*, 2454–2463.

(39) de Vries, A. H.; Chandrasekhar, I.; van Gunsteren, W. F.; Hünenberger, P. H. *J. Phys. Chem. B* **2005**, *109*, 11643–11652.

(40) Darden, T.; York, D.; Pedersen, L. *J. Chem. Phys.* **1993**, *98*, 10089–10092.

(41) Essmann, U.; Perera, L.; Berkowitz, M. L.; Darden, T.; Lee, H.; Pedersen, L. G. *J. Chem. Phys.* **1995**, *103*, 8577–8593.

(42) Tironi, I. G.; Sperb, R.; Smith, P. E.; van Gunsteren, W. F. *J. Chem. Phys.* **1995**, *102*, 5451–5459.

(43) Anézo, C.; de Vries, A. H.; Höltje, H.-D.; Tieleman, D. P.; Marrink, S.-J. *J. Phys. Chem. B* **2003**, *107*, 9424–9433.

(44) Tieleman, D. P.; Marrink, S.-J.; Berendsen, H. J. C. *Biochim. Biophys. Acta* **1997**, *1331*, 235–270.

(45) van der Rest, M. E.; Kamminga, A. H.; Nakano, A.; Anraku, Y.; Poolman, B.; Konings, W. N. *Microbiol. Rev.* **1995**, *59*, 304–322.

(46) Tattrie, N. H.; Bennett, J. R.; Cyr, R *Can. J. Biochem* **1968**, *46*, 819–824.

(47) Kučerka, N.; Liu, Y.; Chu, N.; Petrache, H. I.; Tristram-Nagle, S.; Nagle, J. F. *Biophys. J.* **2005**, *88*, 2626–2637.

(48) Kučerka, N.; Tristram-Nagle, S.; Nagle, J. F. *J. Membr. Biol.* **2005**, *208*, 193–202.

(49) van der Spoel, D.; Lindahl, E.; Hess, B.; Groenhof, G.; Mark, A. E.; Berendsen, H. J. C. *J. Comput. Chem.* **2005**, *26*, 1701–1718.

(50) Berendsen, H. J. C.; Postma, J. P. M.; van Gunsteren, W. F.; DiNola, A.; Haak, J. R. *J. Chem. Phys.* **1984**, *81*, 3684–3690.

(51) Mabrey, S.; Sturtevant, J. M. *Proc. Natl. Acad. Sci. U.S.A.* **1976**, *73*, 3862–3866.

(52) Davis, P. J.; Fleming, B. D.; Coolbear, K. P.; Keough, K. M. W. *Biochemistry* **1981**, *20*, 3633–3636.

(53) Huang, C. H.; Lapides, J. R.; Levin, I. W. *J. Am. Chem. Soc.* **1982**, *104*, 5926–5930.

(54) Lewis, R. N. A. H.; Sykes, B. D.; McElhaney, R. N. *Biochemistry* **1988**, *27*, 880–887.

(55) Hess, B.; Bekker, H.; Berendsen, H. J. C.; Fraaije, J. G. E. M. *J. Comput. Chem.* **1997**, *18*, 1463–1472.

(56) Berendsen, H. J. C.; Postma, J. P. M.; van Gunsteren, W. F.; Hermans, J. Interaction models for water in relation to protein hydration. In *Intermolecular Forces*; Pullman, B., Ed.; Reidel: Dordrecht, The Netherlands, 1981; pp 331−342.

(57) Miyamoto, S.; Kollman, P. A. *J. Comput. Chem.* **1992**, *13*, 952–962.

(58) Heinz, T. N.; van Gunsteren, W. F.; Hünenberger, P. H. *J. Chem. Phys.* **2001**, *115*, 1125–1136.

(59) Rawicz, W.; Olbrich, K. C.; McIntosh, T.; Needham, D.; Evans, E. *Biophys. J.* **2000**, *79*, 328–339.

(60) Tristram-Nagle, S.; Petrache, H. I.; Nagle, J. F. *Biophys. J.* **1998**, *75*, 917–925.

(61) Binder, H.; Gawrisch, K. *J. Phys. Chem. B* **2001**, *105*, 12378–12390.

(62) Marrink, S.-J.; Mark, A. E. *J. Phys. Chem. B* **2001**, *105*, 6122–6127.

(63) Simon, S. A.; McIntosh, T. J. *Methods Enzymol.* **1986**, *127*, 511–521.

(64) Kučerka, N.; Tristram-Nagle, S.; Nagle, J. F. *Biophys. J.* **2006**, *90*, L83–L85.

(65) Petrache, H. I.; Dodd, S. W.; Brown, M. F *Biophys. J.* **2000**, *79*, 3172–3192.

(66) Douliez, J.-P.; Léonard, A.; Dufourc, E. J. *Biophys. J.* **1995**, *68*, 1727–1739.

(67) Seelig, A.; Seelig, J. *Biochemistry* **1977**, *16*, 45–50.

(68) Seelig, J.; Waespe-Šarčević, N. *Biochemistry* **1978**, *17*, 3310–3315.

(69) Perly, B.; Smith, I. C. P.; Jarrell, H. C. *Biochemistry* **1985**, *24*, 1055–1063.

(70) Snyder, R. G.; Strauss, H. L.; Elliger, C. A. *J. Phys. Chem.* **1982**, *86*, 5145–5150.

(71) Mendelsohn, R.; Senak, L. Quantitative determination of conformational disorder in biological membranes by FTIR spectroscopy. In *Biomolecular spectroscopy*; Clark, R. J. H., Hester, R. E., Eds.; Wiley: New York, 1993; pp 339−380.

(72) Cates, D. A.; Strauss, H. L.; Snyder, R. G. *J. Phys. Chem.* **1994**, *98*, 4482–4488.

(73) Moss, G. P. *Pure Appl. Chem.* **1996**, *68*, 2193–2222.

(74) Casal, H. L.; McElhaney, R. N. *Biochemistry* **1990**, *29*, 5423–5427.

(75) Senak, L.; Davies, M. A.; Mendelsohn, R. *J. Phys. Chem.* **1991**, *95*, 2565–2571.

(76) Tuchtenhagen, J.; Ziegler, W.; Blume, A. *Eur. Biophys. J.* **1994**, *23*, 323–335.

(77) Chia, N.-C.; Mendelsohn, R. *Biochim. Biophys. Acta* **1996**, *1283*, 141–150.

(78) Büldt, G.; Gally, H. U.; Seelig, A.; Seelig, J.; Zaccai, G. *Nature* **1978**, *271*, 182–184.

(79) Borle, F.; Seelig, J. *Biochim. Biophys. Acta* **1983**, *735*, 131–136.

(80) Ulrich, A. S.; Volke, F.; Watts, A. *Chem. Phys. Lipids* **1990**, *55*, 61–66.

(81) Ulrich, A. S.; Watts, A *Biophys. J.* **1994**, *66*, 1441–1449.

(82) Lairión, F.; Filler, R.; Disalvo, E. A. *Colloids Surf., B* **2002**, *25*, 369–371.

(83) Lewis, R. N. A. H.; Pohle, W.; McElhaney, R. N. *Biophys. J.* **1996**, *70*, 2736–2746.

(84) Gawrisch, K.; Ruston, D.; Zimmerberg, J.; Parsegian, V. A.; Rand, R. P.; Fuller, N *Biophys. J.* **1992**, *61*, 1213–1223.

(85) Chandrasekhar, I.; Oostenbrink, C.; van Gunsteren, W. F. *Soft Mater.* **2004**, *2*, 27–45.

(86) Chiu, S.-W.; Clark, M.; Balaji, V.; Subramaniam, S.; Scott, H. J.; Jakobsson, E. *Biophys. J.* **1995**, *69*, 1230–1245.

(87) Rosso, L.; Gould, I. R. *J. Comput. Chem.* **2008**, *29*, 24–37.

(88) Åman, K.; Lindahl, E.; Edholm, O.; Håkansson, P.; Westlund, P.-O. *Biophys. J.* **2003**, *84*, 102–115.

(89) Chiu, S.-W.; Clark, M. M.; Jakobsson, E.; Subramaniam, S.; Scott, H. L. *J. Phys. Chem. B* **1999**, *103*, 6323–6327.

(90) Mashl, R. J.; Scott, H. L.; Subramaniam, S.; Jakobsson, E. *Biophys. J.* **2001**, *81*, 3005–3015.

(91) Wong, P. T. T.; Mantsch, H. H. *Chem. Phys. Lipids* **1988**, *46*, 213–224.

(92) Hübner, W.; Blume, A. *Chem. Phys. Lipids* **1998**, *96*, 99–123.

(93) Pearson, R. H.; Pascher, I. *Nature* **1979**, *281*, 499–501.

(94) Rand, R. P.; Parsegian, V. A. *Biochim. Biophys. Acta* **1989**, *988*, 351–376.

(95) Smaby, J. M.; Momsen, M. M.; Brockman, H. L.; Brown, R. E. *Biophys. J.* **1997**, *73*, 1492–1505.

(96) Lewis, B. A.; Engelman, D. M. *J. Mol. Biol.* **1983**, *166*, 211–217.

(97) Gruner, S. M.; Tate, M. W.; Kirk, G. L.; So, P. T.; Turner, D. C.; Keane, D. T.; Tilcock, C. P.; Cullis, P. R. *Biochemistry* **1988**, *27*, 2853–2866.

(98) Pabst, G.; Rappolt, M.; Amenitsch, H.; Laggner, P. *Phys. Rev. E: Stat. Phys., Plasmas, Fluids, Relat. Interdiscip. Top.* **2000**, *62*, 4000–4009.

(99) De Young, L. R.; Dill, K. A. *Biochemistry* **1988**, *27*, 5281–5289.

(100) Mills, T. T.; Toombes, G. E.; Tristram-Nagle, S.; Smilgies, D. M.; Feigenson, G. W.; Nagle, J. F. *Biophys. J.* **2008**, *95*, 669–681.

(101) Balgavý, P.; Dubničková, M.; Kučerka, N.; Kiselev, M. A.; Yaradaikin, S. P.; Uhríková, D. *Biochim. Biophys. Acta* **2001**, *1512*, 40–52.

(102) Lis, L. J.; McAlister, M.; Fuller, N.; Rand, R. P.; Parsegian, V. A. *Biophys. J.* **1982**, *37*, 657–666.

(103) Wiener, M. C.; White, S. H. *Biophys. J.* **1992**, *61*, 434–447.

(104) Janiak, M. J.; Small, D. M.; Shipley, G. G. *J. Biol. Chem.* **1979**, *254*, 6068–6078.

(105) Büldt, G.; Gally, H. U.; Seelig, J.; Zaccai, G. *J. Mol. Biol.* **1979**, *134*, 673–679.

(106) Hyslop, P. A.; Morel, B.; Sauerheber, R. D. *Biochemistry* **1990**, *29*, 1025–1038.

(107) Koenig, B. W.; Strey, H. H.; Gawrisch, K. *Biophys. J.* **1997**, *73*, 1954–1966.

(108) Petrache, H. I.; Tristram-Nagle, S.; Nagle, J. F. *Chem. Phys. Lipids* **1998**, *95*, 83–94.

(109) Thurmond, R. L.; Dodd, S. W.; Brown, M. F. *Biophys. J.* **1991**, *59*, 108–113.

(110) Nagle, J. F.; Zhang, R.; Tristram-Nagle, S.; Sun, W.; Petrache, H. I.; Suter, R. M. *Biophys. J.* **1996**, *70*, 1419–1431.

(111) Kučerka, N.; Kiselev, M. A.; Balgavý, P. *Eur. Biophys. J.* **2004**, *33*, 328–334.

(112) Moore, P. B.; Lopez, C. F.; Klein, M. L *Biophys. J.* **2001**, *81*, 2484–2494.

(113) Lopez, C. F.; Nielsen, S. O.; Klein, M. L.; Moore, P. B. *J. Phys. Chem. B* **2004**, *108*, 6603–6610.

(114) Heller, H.; Schaefer, M.; Schulten, K. *J. Phys. Chem.* **1993**, *97*, 8343–8360.

(115) de Joannis, J.; Jiang, Y.; Yin, F.; Kindt, J. T. *J. Phys. Chem. B* **2006**, *110*, 25875–25882.

(116) Hofsäβ, C.; Lindahl, E.; Edholm, O. *Biophys. J.* **2003**, *84*, 2192–2206.

(117) Jójárt, B.; Martinek, T. A. *J. Comput. Chem.* **2007**, *28*, 2051–2058.

(118) Patra, M. *Eur. Biophys. J.* **2005**, *35*, 79–88.

(119) Zubrzycki, I. Z.; Xu, Y.; Madrid, M.; Tang, P. *J. Chem. Phys.* **2000**, *112*, 3437–3441.

(120) Pasenkiewicz-Gierula, M.; Takaoka, Y.; Miyagawa, H.; Kitamura, K.; Kusumi, A. *Biophys. J.* **1999**, *73*, 1228–1240.

(121) Tieleman, D. P.; Berendsen, H. J. C. *J. Chem. Phys.* **1996**, *105*, 4871–4880.

(122) Repáková, J.; Čapková, P.; Holopainen, J. M.; Vattulainen, I. *J. Phys. Chem. B* **2004**, *108*, 13438–13448.

(123) Chandrasekhar, I.; Bakowies, D.; Glättli, A.; Hünenberger, P.; Pereira, C.; van Gunsteren, W. F. *Mol. Simulat.* **2005**, *31*, 543–548.

(124) Gurtovenko, A. A.; Patra, M.; Karttunen, M.; Vattulainen, I. *Biophys. J.* **2004**, *86*, 3461–3472.

(125) Sonne, J.; Jensen, M. O.; Hansen, F. Y.; Hemmingsen, L.; Peters, G. H. *Biophys. J.* **2007**, *92*, 4157–4167.

(126) Leekumjorn, S.; Sum, A. K. *Biophys. J.* **2006**, *90*, 3951–3965.

CT900487A